Supporting Information

PtCu nanoalloy loaded on sulfur-doped porous g-C$_3$N$_4$ for electrocatalytic hydrogen evolution

Can Chang[a], Jicheng Wu[a], Dandan Wu[a],*, Guojian Jiang[a,b,c,d,e,f],*, Xiaowei Xu[a], Shufang Chang[a]

[a]School of Materials Science and Engineering, Shanghai Institute of Technology, 100 Haiquan Road, Shanghai 201418, R. P. China.

[b]State Key Laboratory of Urban Water Resource and Environment, Harbin Institute of Technology, Harbin 150090, P. R. China.

[c]State Key Laboratory of Crystal Materials, Shandong University, Jinan, Shandong, 250100, P. R. China.

[d]Infrared and Low Temperature Plasma Key Laboratory of Anhui Province, college of Electronic Countermeasures, NUDT, Hefei 230037, P. R. China.

[e]State Key Laboratory of Mineral Processing, Beijing 102628, P. R. China.

[f]State Key Lab Advanced Metals and Materials, Beijing 100083, P. R. China.

Corresponding author: wdan1008@163.com

Materials

The $H_2PtCl_6 \cdot 6H_2O$, $CuCl_2 \cdot 2H_2O$, ethylene glycol and formaldehyde were purchased from Sinopharm Chemical Reagent Co. Ltd. The Nafion (5 wt %) was obtained from Sigma-Aldrich Co. The commercial 20 wt% Pt/C catalysts were obtained from momolab Co. Other reagents were analytical reagent grade. Deionized water was used throughout the experiments.

Characterizations

The crystalline structure of the sample was characterized using the Dutch X'Pert Pro MPD X-ray diffractometer in 2θ mode within the range of 10° to 80° at a scanning rate of $2(°) \cdot min^{-1}$, employing Cu Kα radiation. Surface composition and chemical states of the catalyst were investigated through X-ray photoelectron spectroscopy (XPS) using Al Kα radiation (1486 eV) as a probe on the Thermo Scientific K-Alpha. Characterization of the catalyst was performed using transmission electron microscopy (TEM), high-resolution transmission electron microscopy (HRTEM), high-angle annular dark-field scanning transmission electron microscopy (HAADF-STEM), and energy-dispersive X-ray spectroscopy (EDS) at an accelerating voltage of 200 kV with the JEOL JEM 2100F transmission electron microscope.

Electrochemical measurements

All electrochemical measurements were conducted on the CHI 760E electrochemical workstation (Shanghai CH Instruments Co., Ltd.). In a N_2-saturated 0.5 M H_2SO_4 solution, traditional three-electrode systems were employed for electrochemical experiments. The glassy carbon electrode loaded with the catalyst served as the working electrode, a saturated calomel electrode was used as the reference electrode, and a graphite rod acted as the counter electrode. Prior to testing, cyclic voltammetry (CV) activation was performed. Polarization curves were obtained through linear sweep voltammetry (LSV) with a scan rate of 2 mV·s^{-1}, and the testing potential range was -0.7 V ~ -0.1 V (vs.SCE). All test potentials were converted relative to the reversible hydrogen electrode (RHE) using the formula:

$$E(vs.RHE) = E(vs.SCE) + 0.0591 \times pH + 0.2412$$

No iR compensation applied to any potential. In an N_2-saturated solution, the stability test for the hydrogen evolution reaction (HER) at a current density of 10 mA·cm^{-2} was conducted using the chronopotentiometry method. By measuring CV curves at different scan rates (20, 40, 60, 80, 100 mV s^{-1}) between 0.2 ~ 0.3V (vs RHE), the capacitance (C_{dl}) in the non-Faradaic region was calculated, and ECSA (electrochemical active surface area) was determined through Cdl. Electrochemical impedance spectroscopy (EIS) was recorded in the range of 0.01Hz to 100kHz at an overpotential of 100mV for evaluating the dynamics of the electrochemical reaction.

TOF calculation

The formula for calculating TOF based on the exchange current density(j_0) is as follows:

$$TOF_0 = \frac{j_0 \times S}{2F \times M}$$

Where, the j_0 is the exchange current density, S is the area of the modified Electrode (0.0707cm^{-2}), F is the Faraday's constant and M is the number of moles of Pt in the catalysts.
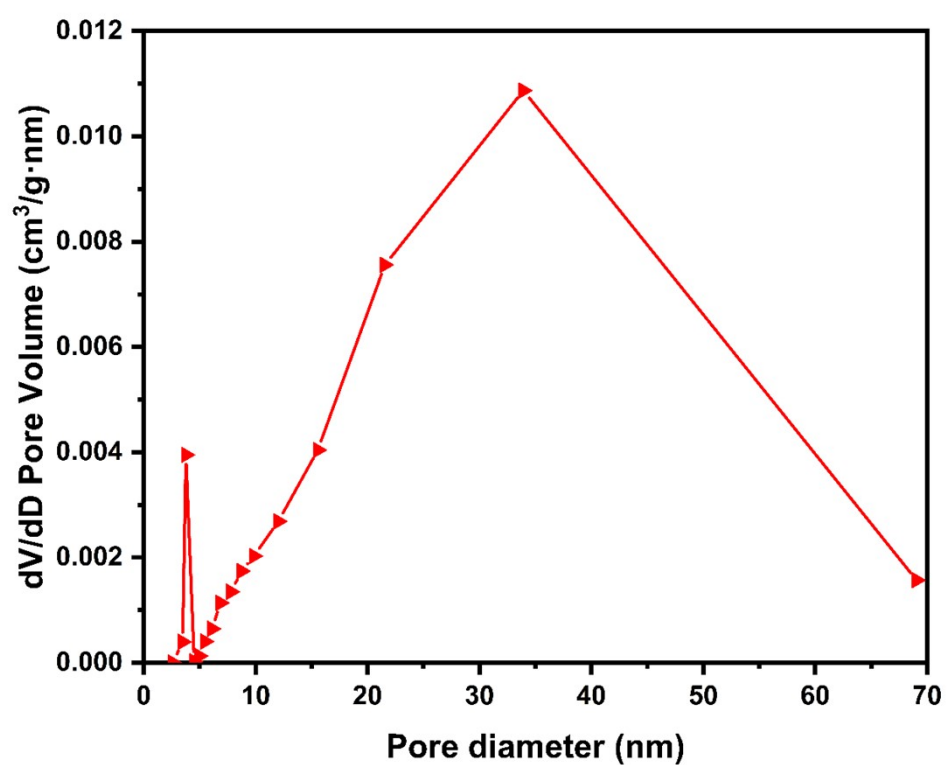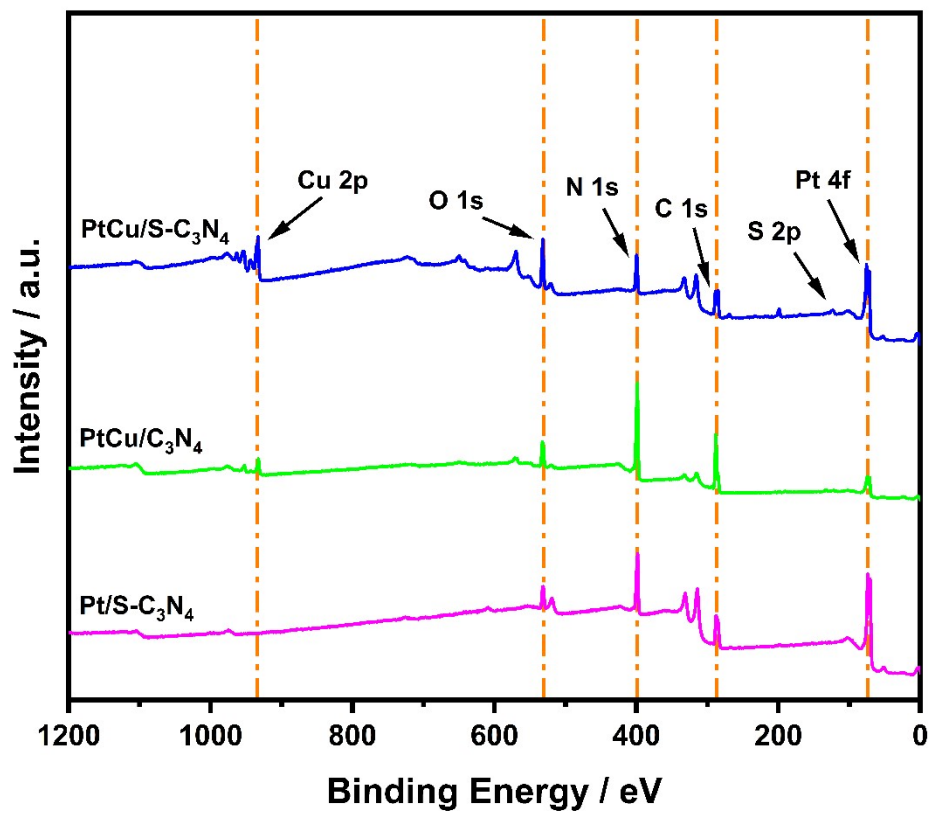
Fig. S1 The pore volume distribution of S-C$_3$N$_4$.
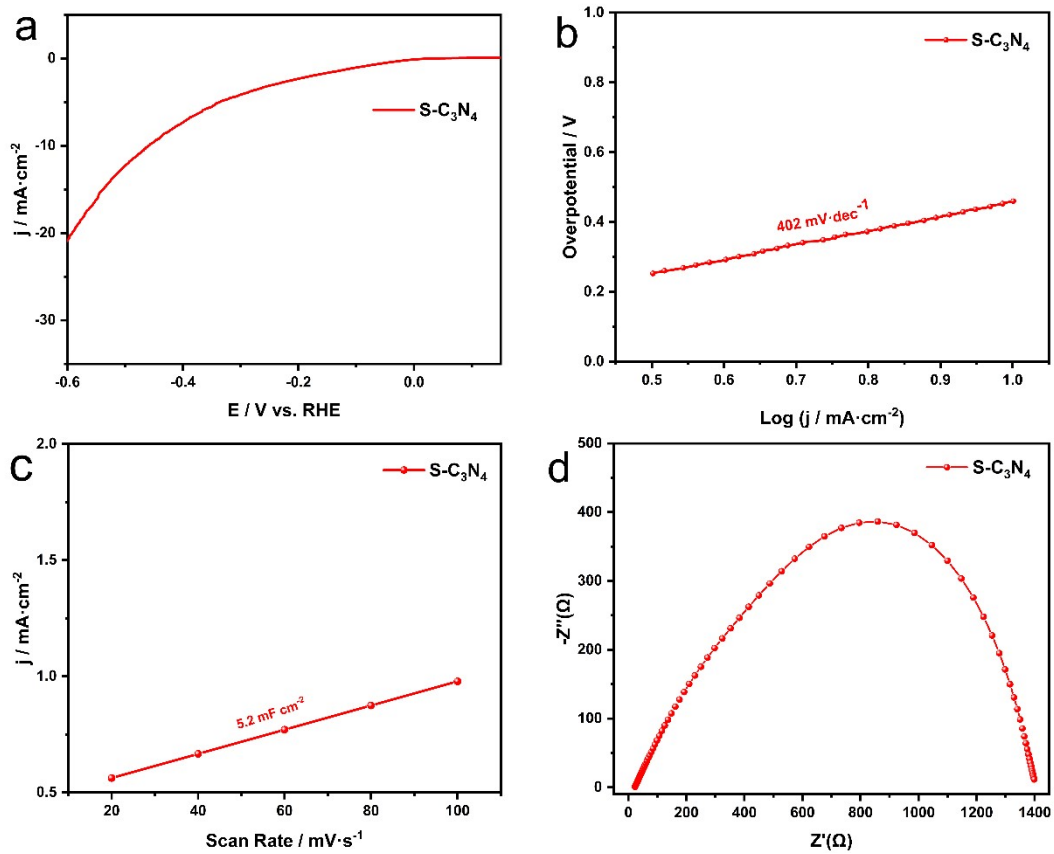
Fig. S2 The full XPS spectrum of the prepared catalyst.

Fig. S3 The Electrocatalytic performance of S-C$_3$N$_4$. (a) LSV curve in N$_2$ saturated 0.5 H$_2$SO$_4$, (b) the Tafel slope, (c) the double-layer capacitance (C$_{dl}$), (d) Nyquist plots at an overpotential of @100 mV.
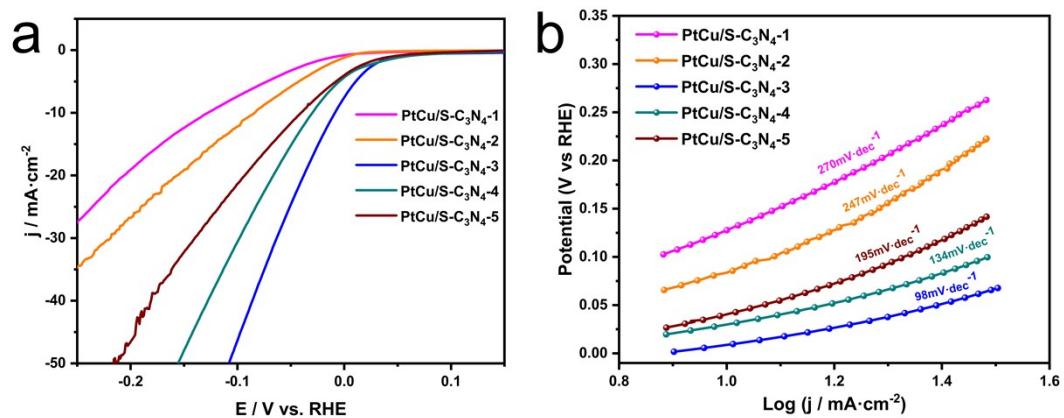
Fig. S4 The LSV curves of different contents of Pt (a) for PtCu/S-C$_3$N$_4$ in N$_2$ saturated 0.5 H$_2$SO$_4$，(b) the Tafel slope of PtCu/S-C$_3$N$_4$-1, PtCu/S-C$_3$N$_4$-2, PtCu/S-C$_3$N$_4$-3, PtCu/S-C$_3$N$_4$-4, PtCu/S-C$_3$N$_4$-5.
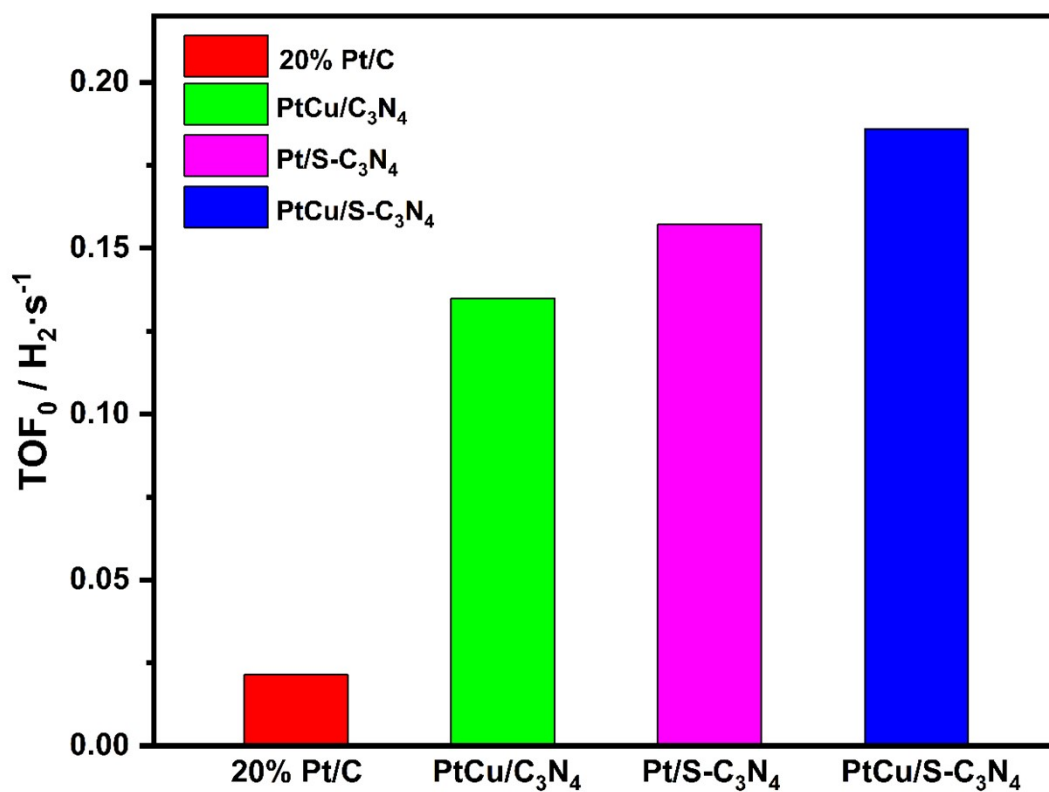
Fig. S5 The turnover frequency (TOF_0) of 20% Pt/C, PtCu/C_3N_4, Pt/S-C_3N_4, PtCu/S-C_3N_4.
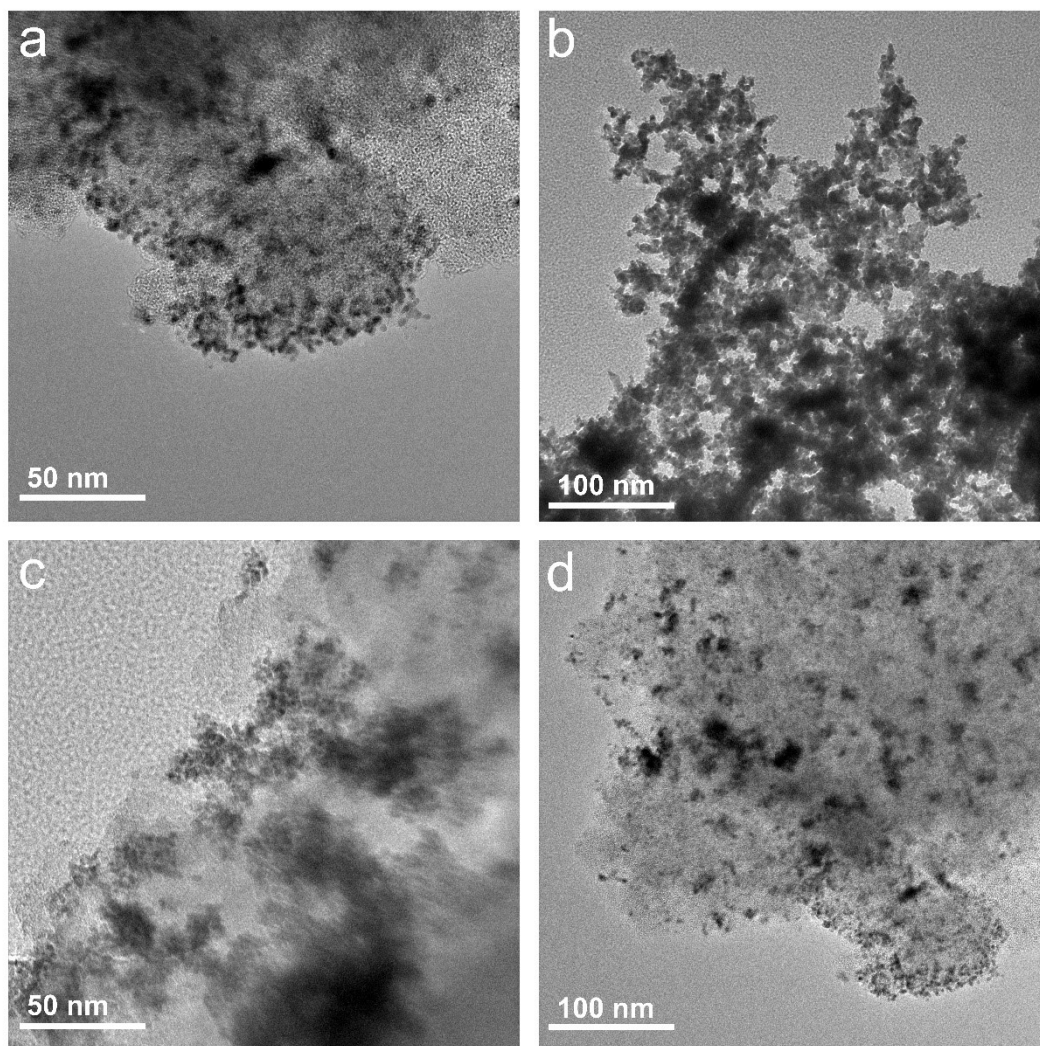
Fig. S6 The TEM image of 20 % Pt/C before (a) and after (b) HER test，PtCu/S-C$_3$N$_4$ before (c) and after (d) HER test.

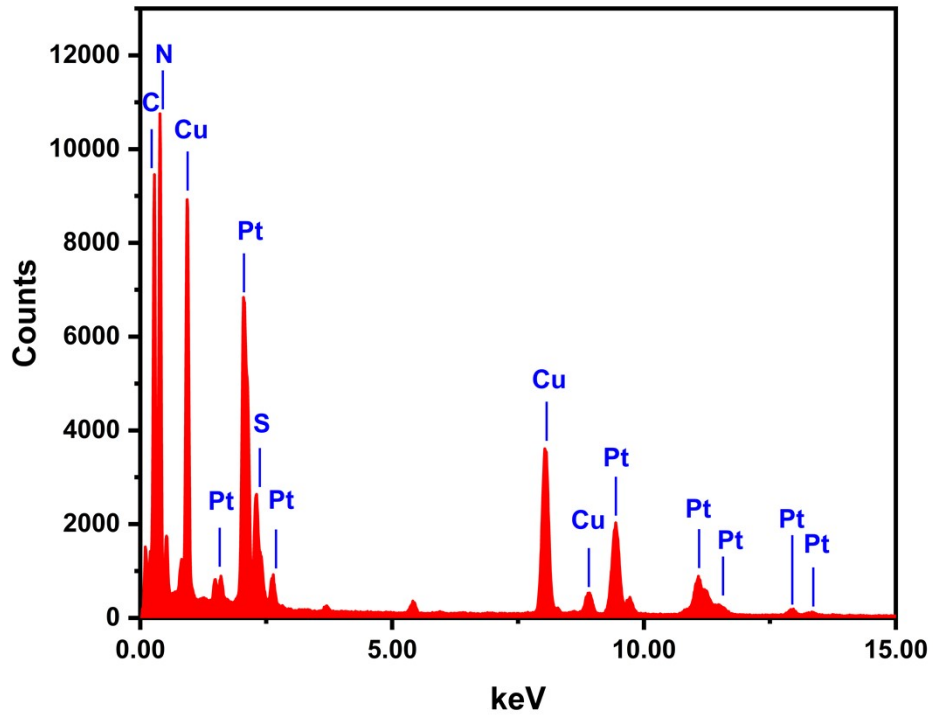**Fig. S7** The EDS corresponding to Figure 2f.

Table. S1 The Pt content of as-prepared catalysts.

Catalysts	Raw materials C_3N_4 (mg)	Raw materials Pt^{4+} (mL)	Raw materials Cu^{2+} (mL)	Cu content (wt%)	Pt content (wt%)
PtCu/S-C$_3$N$_4$-1	50	1	5	5.8	1.8
PtCu/S-C$_3$N$_4$-2	50	2.5	5	5.7	4.4
PtCu/S-C$_3$N$_4$-3	50	5	5	5.4	8.4
PtCu/S-C$_3$N$_4$-4	50	7.5	5	5.2	12.1
PtCu/S-C$_3$N$_4$-5	50	10	5	5	15.5
PtCu/C$_3$N$_4$	50	5	5	5.4	8.4
Pt/S-C$_3$N$_4$	50	5	0	0	8.8

Table. S2 The HER performance of the prepared catalysts.

Catalysts	η_{10} (mV)	tafel slope (V·dec^{-1})	j_0 (mA·cm^{-2})	TOF (s^{-1})
PtCu/S-C$_3$N$_4$	10	98	7.72	0.186
Pt/S-C$_3$N$_4$	15	133	6.82	0.157
PtCu/C$_3$N$_4$	21	105	5.59	0.134
20%Pt/C	35	68	2.09	0.021
S-C$_3$N$_4$	460	402	0.127	—

Table. S3 Summary of recently reported HER electrocatalysts in different electrolytes.

Catalysts	Electrolyte	Overpotential at 10 mA·cm^{-2}	Tafel slope (mV·dec^{-1})	References
PtCu/S-C$_3$N$_4$	0.5M H$_2$SO$_4$	10	98	This work
Pt-C$_3$N$_4$/rGO	0.5M H$_2$SO$_4$	22	30	Int.J.Hydrogen.Energy,2019,29,31121-31128
Ru-C$_3$N$_4$/rGO	0.5M H$_2$SO$_4$	80	56	ChemSusChem,2018, 11, 130-136
Pt/GP-o-300	1M KOH	144	75.9	J.Electroanal.Chem.,2023,939,117476
Pt/Ti$_3$C$_2$Tx-rGO$_{3D}$	0.1 M KOH	41	28	FULLER.NANOTUB.CAR.N.,2023,31,130-135
n-PdCu@NDCDs	0.5M H$_2$SO$_4$	44	88	New J. Chem., 2023, 47, 14355
DA-Pt (1 : 1)	0.5M H$_2$SO$_4$	17	29.1	New J. Chem., 2023,47, 10273
PtNi-NC	0.5M H$_2$SO$_4$	30	27	Sci.China.Mater.,2023,66(4):1389−1397
Fe$_1$Pt$_3$-MoS$_2$	0.5M H$_2$SO$_4$	59	38	Ionics,2023,29,871–875
Co@CNTs|Ru	1M KOH	10	37.8	Nano-Micro.Lett.,2022,14:186
PtNi@La-CNFs	1M KOH	32	51	Int.J.Hydrogen.Energy,2022,47,2423-2432
O-Ti$_{50}$Ni$_{30}$Pt$_{20}$/CNT	1M KOH	21	25.7	J.Mater.Chem.C.,2022,10, 15177
	0.5M H$_2$SO$_4$	36	28.7	
Ru@S/N/CNT	1M KOH	9	37	New J. Chem., 2022, 46, 15804
	0.5M H$_2$SO$_4$	68	44	
CoPt$_3$@NC	1M KOH	65	67	Electrochemical Science Advances,2022,2, 1-9
Pt–PNWs	0.5M H$_2$SO$_4$	27	24.3	Bull.Korean.Chem.Soc.,2022,43,1111–1117.
Pt-doped WS$_2$	0.5M H$_2$SO$_4$	60	40	J.Appl.Electrochem.,2022.52,499–507

Table. S4 The corresponding element content of Fig.S7

Element	Atom%
C	53.11
N	34.26
S	1.46
Pt	4.31
Cu	6.85